REVIEW

Quantum information processing by nuclear magnetic resonance on quadrupolar nuclei

By João Teles[1,*], Eduardo R. deAzevedo[2], Jair C. C. Freitas[3],
Roberto S. Sarthour[4], Ivan S. Oliveira[4] and Tito J. Bonagamba[2]

[1]*Departamento de Ciências da Natureza, Matemática e Educação,*
Universidade Federal de São Carlos, 13600-970, Araras, São Paulo, Brazil
[2]*Instituto de Física de São Carlos, Universidade de São Paulo, Caixa Postal*
369, 13560-970, São Carlos, São Paulo, Brazil
[3]*Departamento de Física, Universidade Federal do Espírito Santo, 29075-910,*
Vitória, Espírito Santo, Brazil
[4]*Centro Brasileiro de Pesquisas Físicas, 22290-180, Rio de Janeiro, Brazil*

Nuclear magnetic resonance is viewed as an important technique for the implementation of many quantum information algorithms and protocols. Although the most straightforward approach is to use the two-level system composed of spin $\frac{1}{2}$ nuclei as qubits, quadrupolar nuclei, which possess a spin greater than $\frac{1}{2}$, are being used as an alternative. In this study, we show some unique features of quadrupolar systems for quantum information processing, with an emphasis on the ability to execute efficient quantum state tomography (QST) using only global rotations of the spin system, whose performance is shown in detail. By preparing suitable states and implementing logical operations by numerically optimized pulses together with the QST method, we follow the stepwise execution of Grover's algorithm. We also review some work in the literature concerning the relaxation of pseudo-pure states in spin $\frac{3}{2}$ systems as well as its modelling in both the Redfield and Kraus formalisms. These data are used to discuss differences in the behaviour of the quantum correlations observed for two-qubit systems implemented by spin $\frac{1}{2}$ and quadrupolar spin $\frac{3}{2}$ systems, also presented in the literature. The possibilities and advantages of using nuclear quadrupole resonance experiments for quantum information processing are also discussed.

Keywords: quantum information processing; quantum state tomography;
nuclear magnetic resonance; quadrupolar nuclei

1. Introduction

Among the main results of using nuclear magnetic resonance (NMR) for quantum information processing (QIP), we find that preparation of pseudo-pure states

*Author for correspondence (jteles@cca.ufscar.br).

(PPS), radio frequency (RF) pulse design for logic gate implementation and reading procedures, e.g. quantum state tomography (QST), are handled very well, due mainly to the fine control of the quantum evolution of nuclear spins. Allied to these characteristics are the relatively long relaxation times of nuclear magnetization, which, in the language of QIP, implies that the decoherence times of the nuclear quantum states are lengthy enough to perform the desired unitary evolutions. Nuclei with spin greater than $\frac{1}{2}$ under the quadrupolar interaction provide an alternative means of creating an N-qubit system [1–6]. The main advantages are the use of shorter pulse sequences than those applied to the spin systems in isotropic liquids and the representation of many qubits by only one nuclear species. Naturally, the same high strength of the quadrupolar couplings that enables the use of shorter pulses in quadrupolar systems gives rise to shorter relaxation times, leading to stronger decoherence and dissipation effects. However, this difference in the relaxation of quadrupolar and spin $\frac{1}{2}$ systems arises from the distinct nature of the spin–environment interaction; so these systems can be used as models to investigate the differences in the decoherence and dissipation of quantum systems, in which the system–environment interaction is described by distinct quantum channels. Another characteristic of nuclear spins with strong quadrupolar moments is the possibility of performing QIP by means of nuclear quadrupole resonance (NQR) without using an external magnetic field. As a result of all these possibilities, there are many studies exploring QIP concepts by NMR in quadrupolar systems. The purpose of this study is to review some of the work published in this area and to present new results showing the excellent control over quadrupolar systems achieved by similar RF pulse techniques.

QST is an important tool for characterizing the various stages of a quantum algorithm implementation. The first QST proposal for NMR was put forward by Chuang *et al.* [7] and further improved by Long *et al.* [8]. In those works, the authors proposed a technique for QST in heteronuclear coupled spin $\frac{1}{2}$ systems. In heteronuclear systems, non-selective RF pulses can act on each nucleus separately. Such pulses generate individual spin rotations which, by means of specific pulse combinations, make it possible to project all the components needed to expand the system's density matrix in the NMR measurement operator. In the case of homonuclear spin $\frac{1}{2}$ and quadrupolar systems, non-selective pulses produce only global rotations of all qubits: it is not possible to rotate one qubit state at a time. Therefore, to address the specific qubit states of such systems, several approaches have been proposed to use selective RF pulses to excite specific nuclear transitions [2,3,5,6,9]. However, owing to the long duration of selective pulses, relative to the non-selective ones used in heteronuclear systems, relaxation effects can severely restrict the use of QST methods. This restriction turns out to be more important if the number of spins increases or the spin quantum number is greater than $\frac{1}{2}$, because in these cases, many more selective excitations are necessary to find all the elements of the density matrix [6]. As a way to overcome these limitations, we proposed a QST method using only short non-selective RF pulses with a coherence selection scheme [10]. As a result, many studies involving quadrupolar nuclei could benefit from that method, including research on quadrupolar spin decoherence and relaxation [11–14] and quantum simulation [15]. Section 2 briefly expounds the main concepts regarding PPS and logic gate implementation and QST in high-field NMR of quadrupolar nuclei. To illustrate the fine control obtained,

§2c,d presents the experimental results of the spin $\frac{3}{2}$ quantum state rotations associated with specific irreducible tensor operators and Grover's quantum search algorithm, respectively.

As mentioned earlier, another interesting way of using quadrupolar nuclei for QIP is the NQR technique. Systems of quadrupolar nuclei in a non-vanishing electric field gradient (EFG) have been put forward as candidates for the implementation of QIP in NQR experiments. The pioneering proposal was put forward by Furman et al. [16,17], who used two RF fields applied in different directions and with different phases to remove the degeneracy of the energy levels in pure NQR. The preparation of PPS and the implementation of simple gates (C-NOT, AND, SWAP) were discussed, but no experimental demonstration of this method (which seems to be hard to implement in terms of instrumentation) has been reported so far. More recently, Possa et al. [18] described how circularly polarized RF combined with double quantum excitation can be used to create PPS and implement simple quantum gates in NQR. As these methods are well established in the NQR literature [19–21], the extension of their scope to experiments dealing with QIP sounds quite plausible. Such developments are briefly analysed in §3.

The idea of comparing the relaxation behaviour of two-qubit systems implemented by spin $\frac{1}{2}$ and quadrupolar spin $\frac{3}{2}$ nuclei is discussed in §4. To achieve that, we first describe the relaxation of quadrupolar spin $\frac{3}{2}$ systems in terms of both the more NMR-friendly Redfield formalism [11,22] and quantum channels [13], more familiar in the QIP community [23,24]. Furthermore, the effect of the system–environment interaction on the behaviour of the classical and quantum correlation of spin $\frac{1}{2}$ [25] and spin $\frac{3}{2}$ [14] NMR systems is described, and the origin of the difference in behaviour is discussed.

2. High-field NMR of quadrupolar nuclei

(a) Preparation of initial states

The magnetic states of a nucleus with spin quantum number I in a strong magnetic field $B_0\hat{z}$ correspond to the eigenvalues of the z component of the angular momentum operator, I_z: $I, I-1, \ldots, -I-1, -I$. In such a system, the magnetic states of the nucleus, with spin $I = \frac{1}{2}(2^N - 1)$, can be associated with the logic states of an N-qubit system. Therefore, a two-qubit system can be implemented by a spin $\frac{3}{2}$ nucleus, three qubits by a spin $\frac{7}{2}$ nucleus and so on. In practice, as for the spin $\frac{1}{2}$ systems, the main magnetic field alone is not sufficient for the use of spins $> \frac{1}{2}$ as QIP systems. In order to produce the most general states needed for QIP via NMR, it is necessary to add an interaction whose quantum operator is not a rotation generator. The interaction that performs that function in NMR of nuclei with $I > \frac{1}{2}$ (referred to as quadrupolar nuclei or quadrupolar spin) is the coupling of the nuclear electric quadrupole moment with the EFG at the site of the nucleus, produced by neighbouring electrical charges.

The EFG is described by a second rank tensor whose components correspond to the second derivative of the scalar potential evaluated at the position of the nucleus: $V_{\alpha\beta} = (\partial^2 V/\partial\alpha\partial\beta)_{r=0}$ with $\alpha, \beta = x, y, z$. In the principal axis system
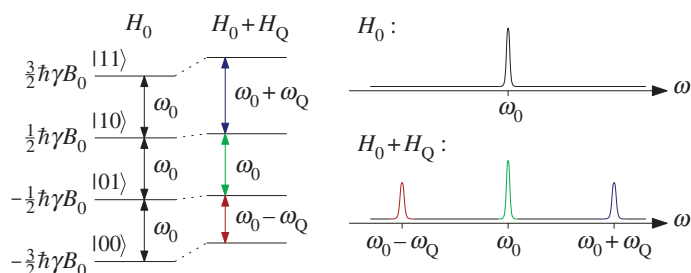
Figure 1. Logical labelling of the spin $\frac{3}{2}$ energy levels without and with the quadrupolar perturbation. The corresponding spectra are illustrated. (Online version in colour.)

(PAS), the symmetrical and traceless tensor $V_{\alpha\beta}$ is null for $\alpha \neq \beta$. The PAS is chosen such that $|V_{zz}| \geq |V_{yy}| \geq |V_{xx}|$ and the following parameters are defined: $eq = V_{zz}$ and $\eta = (V_{xx} - V_{yy})/V_{zz}$. It can then be shown that the quadrupolar Hamiltonian is given by

$$H_Q = \frac{e^2 qQ}{4I(2I-1)} \left[3I_z^2 - I(I+1) + \frac{\eta}{2}(I_+^2 + I_-^2) \right]. \tag{2.1}$$

In cases where the interaction with the static magnetic field B_0 is much stronger than the quadrupolar interaction, only the secular part of H_Q must be considered. Moreover, when the EFG tensor shows axial symmetry ($\eta = 0$), equation (2.1) is further simplified, and the full static Hamiltonian, including the interaction of the main magnetic field B_0, is given by

$$H = H_0 + H_Q = -\hbar \omega_0 I_z + \hbar \frac{\omega_Q}{6}[3I_z^2 - I(I+1)]. \tag{2.2}$$

The coupling parameters are $\omega_0 = \gamma B_0$ and $\omega_Q = (3\,e^2 qQ/4I(2I-1))(3\cos^2\theta - 1)$, where γ is the nuclear gyromagnetic ratio and θ is the angle between the z-axis of the PAS and the main magnetic field B_0. Figure 1 illustrates the energy levels and the spectrum associated with the transitions of a spin $\frac{3}{2}$ nucleus, representing a system of two qubits.

In NMR, the thermal equilibrium state is found in an almost maximum mixture state, where the corresponding density matrix ρ_{eq} deviates little from the normalized identity matrix. However, if it is possible to transform ρ_{eq} into a state of the form

$$\bar{\rho} = \frac{1}{2^N}(1 - q)\mathbf{1} + q|\psi\rangle\langle\psi|, \tag{2.3}$$

then it is possible to perform any quantum computation experiment considering the $|\psi\rangle\langle\psi|$ term. That is because the identity operator is invariant under unitary operations and, consequently, can be neglected. The state created in such a way is called a PPS and the factor q is a real number between 0 and 1 [26,27]. In equation (2.3), only the deviation matrix $\Delta\bar{\rho} = q(|\psi\rangle\langle\psi| - \mathbf{1}/2^N)$ is accessible in NMR experiments, and this is the matrix usually appearing in the experimental results, as happens in this study.

RF pulse sequences, magnetic field gradients and time-average procedures are the main tools in producing experimentally, by NMR, the PPS and logic gates used in the quantum algorithms and protocols. Analytical approximating procedures such as the average Hamiltonian theory [28] or the employment of selective pulses in multiple quantum transitions [29,30] are normally used to produce the effective Hamiltonians that correspond to the unitary operations used in QIP. However, general quantum operations are not always easily obtained by analytical procedures, and numerical strategies can be useful. One important technique is the strongly modulating pulse (SMP) [31], which is used in many QIP implementations, including the Grover's algorithm implementation shown in this study.

(b) Quantum state tomography with hard pulses

Now, a short account will be given of how the QST of quadrupolar nuclei in NMR can be performed exclusively by global rotations of the spin system [10]. Non-selective pulses have the property of performing almost ideal rotations of the spin system. Therefore, it is useful to expand the density operator ρ in a basis formed by irreducible tensor operators [32], which exhibit special properties under rotations:

$$\rho = \sum_{l,m} a_{l,m}\, T_{l,m}(I). \tag{2.4}$$

The $T_{l,m}(I)$ are the irreducible tensor operators of rank l and order m, which depend on the spin quantum number I of the quadrupolar nucleus. In this case, to reconstruct the ρ operator it suffices to determine the coefficients $a_{l,m}$. When short non-selective pulses are applied, the corresponding evolution operator corresponds to the rotation operator R. The $T_{l,m}$ operators transform under rotation in the same way as spherical harmonics:

$$R \cdot T_{l,m} \cdot R^\dagger = \sum_{m'=-l}^{l} D^l_{m',m}\, T_{l,m'}. \tag{2.5}$$

The $D^l_{m',m}$ rotation matrix elements are called the Wigner D-functions [32], defined by $\langle l', m'|R|l,m\rangle = \delta_{l',l} D^l_{m',m}$, where $|l,m\rangle$ are the eigenstates of the angular momentum operator with quantum number l and projection m. We are interested in the NMR case where the axis of rotation is restricted to the x–y plane. Therefore, only two angles are necessary to characterize the pulse action: the phase angle ϕ of the rotation axis with respect to the x-axis and the nutation angle θ that the spin states perform around the rotation axis. Under such conditions, Wigner D-functions can be simplified to

$$D^l_{m',m}(\phi,\theta) = e^{i(m-m')(\phi-\pi/2)}\, d^l_{m',m}(\theta). \tag{2.6}$$

The $d^l_{m',m}(\theta)$ are called the reduced Wigner D-functions [32] and they contain only the dependence on the nutation angle. The pulse phase ϕ appears as an imaginary phase multiplied by the difference between the coherence order before (m), and after (m'), the rotation. This phase dependence will be used to select specific coherences using a temporal coherence selection scheme. The NMR

spectral amplitudes are derived from the expression for the magnetization M in the phasor notation:

$$M(t) = \text{Tr}\{U(t) \cdot \tilde{\rho} \cdot U^\dagger(t) \cdot I_+ e^{i\alpha}\}, \tag{2.7}$$

where $\tilde{\rho} = R \cdot \rho \cdot R^\dagger$ is the rotated density matrix, $U(t)$ is the evolution operator under the free Hamiltonian (2.2) (i.e. without RF perturbation), $I_+ = I_x + I_y$ is the raising operator and α is the detection phase.

By applying equations (2.4)–(2.6) to equation (2.7), the following expression for the nuclear magnetization is obtained:

$$M(t) = \sum_k e^{i\omega_k t} S_k, \tag{2.8}$$

where

$$\omega_k = \frac{E_k - E_{k+1}}{\hbar} \tag{2.9}$$

and the spectral amplitudes

$$S_k = \sum_{l,m} a_{l,m}^* e^{i(1-m)(\phi-\pi/2)+i\alpha} d_{1,m}^l(-\theta)[I_+]_{k,k+1}[T_{l,1}]_{k,k+1}. \tag{2.10}$$

The energies E_k are the eigenstates of the free Hamiltonian. To perform QST on the system, it is necessary to find the unknown amplitudes $a_{l,m}$ from the spectral amplitudes S_k. The index k goes from $m_k = -I$ to $m_k = I - 1$, totalling $2I$ spectral lines. The square brackets in equation (2.10) denote the matrix element of the respective operator. Each S_k has, generally, contributions from all $a_{l,m}$ coefficients, which form a set of $I(2I+3)$ elements. Therefore, to determine all $a_{l,m}$, it is necessary to apply additional rotations by using new RF pulses, in which a suitable choice of the experimental parameters (α, θ and ϕ) allows the reconstruction of the density matrix. To this end, a temporal coherence selection scheme is applied. In such a scheme, the NMR experiment is repeated N times with a different RF pulse phase ϕ_n and receiver phase α_n for each repetition. The resulting amplitudes are averaged in the form

$$\bar{S}_k = \frac{1}{N} \sum_{n=0}^{N-1} S_k(\phi_n, \alpha_n). \tag{2.11}$$

By choosing the phase angles and the number of averages to satisfy the following equations:

$$\left.\begin{aligned}
\phi_n &= \frac{2\pi n}{N} + \frac{\pi}{2}, \\
\alpha_n &= \frac{2\pi n(m'-1)}{N} \\
N &\geq 2I + m' + 1,
\end{aligned}\right\} \tag{2.12}$$

and

it can be shown [10] that equation (2.11) reduces to

$$\bar{S}_k(m') = \sum_{l=l'}^{2I} a_{lm'}^* d_{1,m'}^l(-\theta)[A_l]_{k,k+1}, \tag{2.13}$$

where $l' = \max(1, m')$. Now, the averaged signal $\bar{S}_k$ depends on only one coherence order, m', which is selected by the phases in equations (2.12). Equation (2.13) corresponds to the linear system

$$\mathbf{A} \cdot \mathbf{x} = \mathbf{b}$$

$$\left.\begin{aligned}
[\mathbf{A}]_{k,l-l'+1} &= [I_+]_{k,k+1}[T_{l,1}]_{k,k+1}, \quad \text{where } k = 1, 2, \ldots, 2I, \\
[\mathbf{x}]_{l-l'+1} &= a^*_{lm'} d^l_{1,m'}(-\theta), \quad \text{where } l = l', l'+1, \ldots, 2I \\
\text{and} \qquad [\mathbf{b}]_k &= \bar{S}_k(m').
\end{aligned}\right\} \tag{2.14}$$

Owing to the linear independent character of the irreducible tensors, equation (2.14) is also linearly independent. Therefore, quadrupolar nuclei can be completely tomographed only with global spin rotations that are performed by short hard RF pulses.

Here, we have focused in the single quadrupolar nucleus system. However, because the maximum nuclear spin quantum number available for NMR experiments is limited, it is convenient that the method be extended to coupled spin systems. Such an extension was already carried out and can be appreciated in Teles *et al.* [10], where, by using the irreducible tensor product, the QST method was applied to a fictitious homonuclear three-spin $\frac{1}{2}$ system.

(c) Irreducible tensor rotation

As discussed in §2b, the reduced Wigner D-functions $d^l_{1,m}(-\theta)$ determine the dependence of the density matrix coherence amplitudes on the nutation angle θ of the non-selective pulses. In order to show this experimentally, SMPs [31] were optimized such that the density matrix was proportional to the irreducible tensor operators T_{lm}. By varying the nutation angle θ of the tomography pulses, it was possible to verify the dependence of the T_{lm} on the respective Wigner D-functions $d^l_{1,m}$. Only the T_{lm} of negative order were considered, which resulted in nine operators to be optimized, because we are dealing with a spin $\frac{3}{2}$ nucleus. The measured experimental fidelities are shown in table 1 and they are based on the Hilbert–Schmidt inner product of operators [23,31]. The fidelity F refers to the calculation with respect to the complete operator, while F' considers only the non-null elements of the corresponding T_{lm} state. It is important to note that as the density operator is Hermitian, the states are proportional to the sum of the tensor operator with its adjoint: $\rho \propto T_{lm} + T^\dagger_{lm} = T_{lm} + (-1)^m T_{l,-m}$.

Equation (2.13), for the selected spectral amplitudes of order m, when considering only one rank, l, reduces to

$$\bar{S}_k(m) = a^*_{lm} d^l_{1,m}(-\theta)[A_l]_{k,k+1}. \tag{2.15}$$

Thus, one can choose a spectral amplitude and monitor its variation as a function of the nutation angle θ. Because this dependence is given by the reduced Wigner D-function $d^l_{1,m}$, this experiment is useful to demonstrate what the less error-dependent angles θ are for the RF pulses performing the QST. Figure 2 presents the experimental data juxtaposed to the $d^l_{1,m}(-\theta)$ theoretical curves for comparison. It is important to note that these results were obtained without any
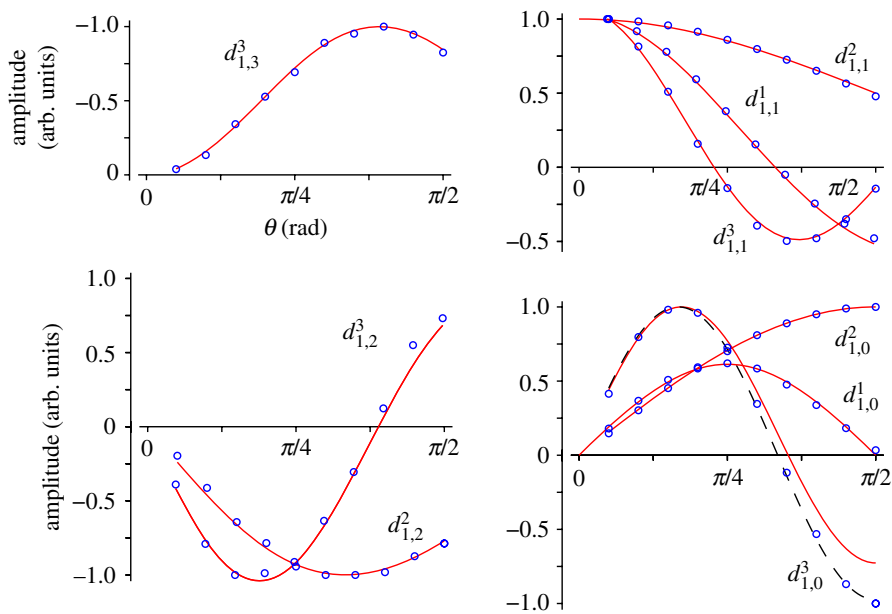
Figure 2. Normalized spectral amplitudes plotted against the nutation angle θ for each irreducible tensor operator of the spin $\frac{3}{2}$ nucleus. Solid lines denote theoretical curves; circles denote experimental data. (Online version in colour.)

Table 1. Experimental fidelities of the states corresponding to the irreducible tensor operators of the spin $\frac{3}{2}$ nucleus.

operator	F	F'
$T_{1,0}$	0.999	0.999
$T_{2,0}$	0.932	0.967
$T_{3,0}$	0.969	0.984
$T_{1,-1} - T_{1,1}$	0.992	0.993
$T_{2,-1} - T_{2,1}$	0.950	0.987
$T_{3,1} - T_{3,-1}$	0.936	0.978
$T_{2,2} + T_{2,-2}$	0.843	0.958
$T_{3,2} + T_{3,-2}$	0.893	0.914
$T_{3,3} - T_{3,-3}$	0.875	0.993

reconstruction process, as for example, by using the linear system (2.14). They correspond directly to the amplitudes obtained from the spectra after application of the RF pulse sequence used to generate the T_{lm} states and after performing the coherence selection. In particular, the states $T_{1,1} + T_{1,1}^{\dagger}$ and $T_{1,0}$ were obtained without the use of SMPs, because the former is proportional to the I_x state, being straightforwardly generated by a hard $\pi/2$ pulse, and the latter is proportional to the thermal equilibrium state I_z. The plots of figure 2 show an excellent agreement between the data and the theoretical curves, especially in the regions of maximum
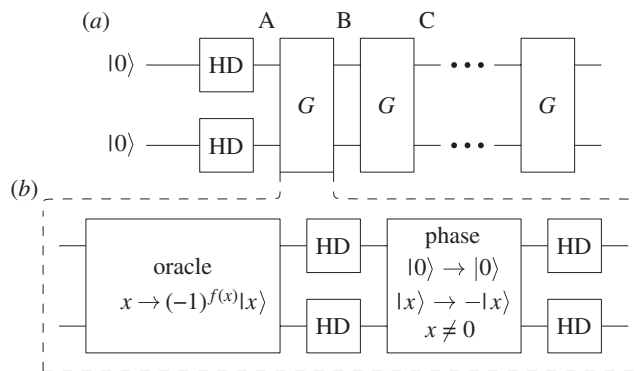
Figure 3. (*a*) Grover's algorithm quantum circuit for two qubits implemented in this study. (*b*) Composition of each Grover operator.

amplitudes. Significant deviation only occurs for θ near $\pi/2$ in the lower right part of the $d_{1,0}^3$ curve. In this case, it was possible to observe the mixture with other ranks. With a high F' fidelity of 0.984, a negligible contribution would be expected from other ranks besides $l = 3$. However, fidelities of 0.166 and 0.053 were found for the experimentally tomographed state $T_{3,0}$ with respect to the theoretical states $T_{1,0}$ and $T_{2,0}$, respectively. Allied to that, there is the fact that the Wigner D-function $d_{1,0}^1$ is very high for angles near $\pi/2$, which accounts for a non-negligible contribution for the nutation curve. The dashed curve in the $d_{1,0}^3$ plot was constructed by taking into account these contributions, showing a good agreement with the experimental data. As the agreement is good, especially in the regions of maximum amplitudes, it can be inferred that there was no significant quadrupolar evolution during the application of the hard RF tomography pulses. This indicates that it is not necessary to employ more involved pulses, using some kind of modulation or self-refocusing strategies, to perform QST with hard non-selective pulses.

(*d*) Grover's algorithm

With the purpose of illustrating the advantages of the QST method using hard pulses, Grover's algorithm [33] was experimentally implemented with five iterations. In order to reconstruct the entire density matrix for many operator repetitions, the reading pulses have to be short enough for spin relaxation to be unimportant.

Grover's algorithm allows an element from an unsorted database of size N to be obtained in a time of order $O(\sqrt{N})$. The polynomial speed-up in the search process represents an advantage over the classical counterpart, $O(N)$. The algorithm belongs to the class of probabilistic quantum algorithms and a detailed description can be found elsewhere [9,23,33–36]. The exposition here is restricted to the description of the two-qubit quantum circuit, which is represented in figure 3. In figure 3*a*, the input state corresponds to $|\psi\rangle = |00\rangle$. Next, the Hadamard gate is applied to the two qubits in order to create the superposition state $|\psi\rangle = \frac{1}{2}(|00\rangle + |01\rangle + |10\rangle + |11\rangle)$. Thereafter, Grover's
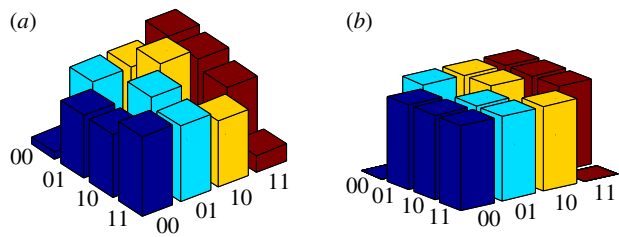
Figure 4. Quantum state tomography of the superposition PPS $|\psi\rangle = \frac{1}{2}(|00\rangle + |01\rangle + |10\rangle + |11\rangle)$ (real part only). (*a*) Experimental and (*b*) theoretical. (Online version in colour.)

Table 2. Numerical fidelities F, RF pulse duration and the number of segments of the SMPs for each optimized Grover operator.

operator	F	duration (µs)	segments
G_{00}	0.988	114.50	5
G_{01}	0.991	163.00	5
G_{10}	0.990	141.39	5
G_{11}	0.984	107.30	5

operator G is repeatedly applied a number of times of order $O(\sqrt{N})$, until the output state shows a high probability of being the correct answer to the problem. In the general case, it may be necessary to use auxiliary qubits to operate on the solution qubit database. Figure 3*b* shows the parts of Grover's operator. It is composed of the oracle operator, O, followed by a phase gate inserted between two Hadamard (HD) gates on each qubit. The oracle function $f(x)$ is responsible for problem solution discrimination. It results in $f(x) = 1$ if x is a solution and $f(x) = 0$ otherwise. It can be shown that the phase operator and the two Hadamard gates correspond to the operator $2|\psi\rangle\langle\psi| - \mathbf{1}$. The functions $f(x)$ used by the oracle and experimentally implemented herein are given by

$$f_y(x) = \begin{cases} 0, & \text{for } x \neq y \\ 1, & \text{for } x = y \end{cases} \tag{2.16}$$

where x and y are any of the four states of the two-qubit system. Therefore, the implemented operation is equivalent to the search process of one among the four functions f_y. The corresponding Grover operators are denoted by G_{00}, G_{01}, G_{10} and G_{11}.

The algorithm was implemented experimentally by the optimization of many steps into one. The superposition state $|\psi\rangle$ was directly created by the SMP method [31] and its QST is shown in figure 4. The experimental fidelity obtained was 0.878. Each Grover operation was also implemented by only one SMP. Table 2 contains the numerical properties of these operations. The experimental QST of the G operators for five iterations is shown in figure 5, where just the results for the operators G_{00} and G_{01} are given. It can be shown that the quantum search algorithm finds the element in the first try for the two-qubit case. Moreover, the algorithm presents a periodic behaviour, where the number of iterations of the G
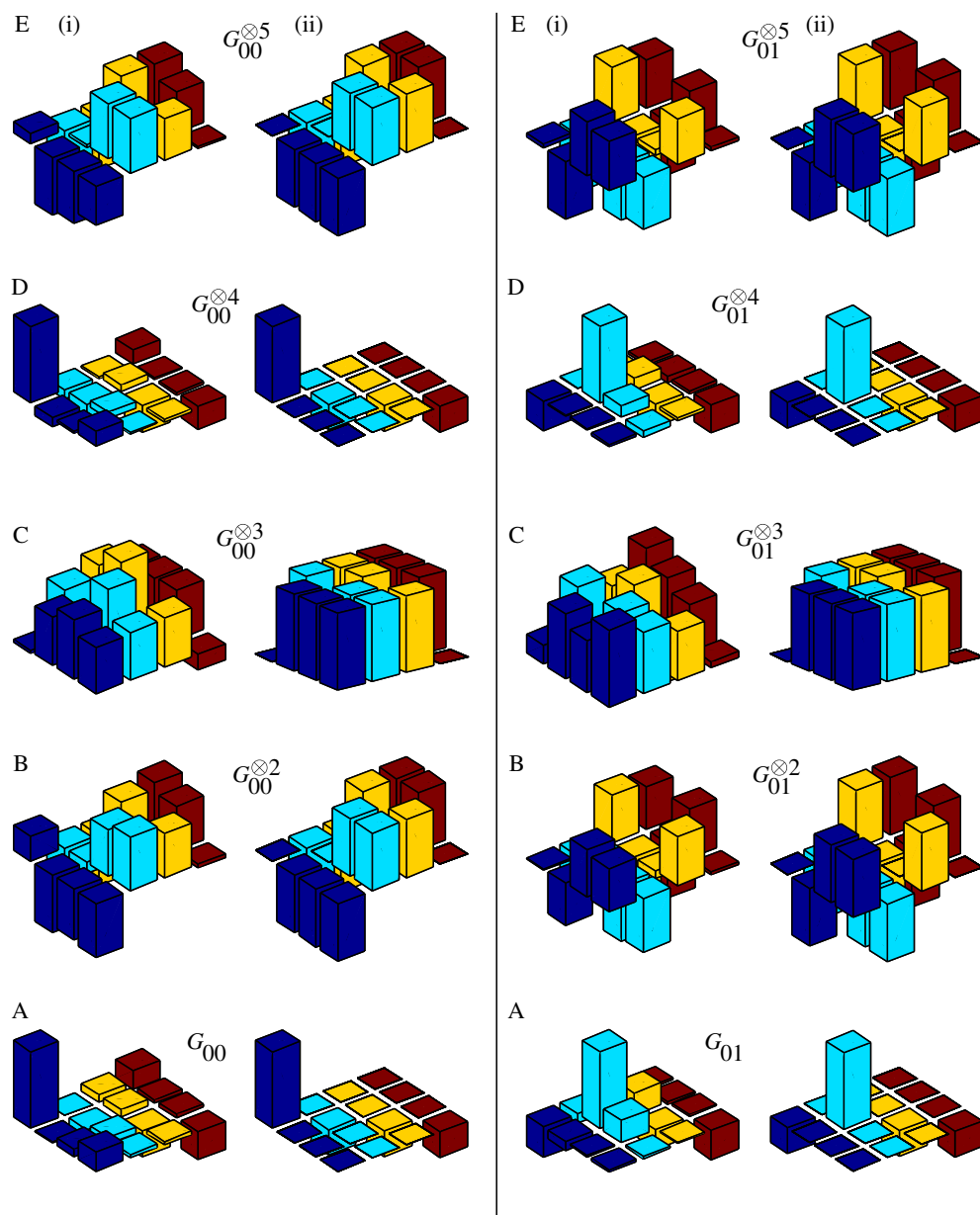
J. Teles et al.

Figure 5. Quantum state tomography of Grover's algorithm for operations G_{00} and G_{01} (real part only). Iterations A to E are represented in figure 3 and table 3. The horizontal axes follow the same convention of figure 4. (i) Experimental and (ii) theoretical. (Online version in colour.)

operator necessary for a new maximum probability is 3. This behaviour is clearly observed in the experimental results of figure 5. The measured quantum state fidelities for each iteration are shown in table 3. Some of the lower state fidelities are attributed mainly to the RF pulse imperfections and the time delays intrinsic to the hardware.

Table 3. Experimental quantum state fidelities obtained from the quantum state tomography of each iteration of the Grover operators.

iteration	G_{00}	G_{01}	G_{10}	G_{11}
A	0.964	0.957	0.932	0.895
B	0.890	0.891	0.833	0.960
C	0.887	0.848	0.819	0.842
D	0.966	0.928	0.872	0.932
E	0.897	0.877	0.788	0.943

3. Nuclear quadrupole resonance studies

NQR is a technique closely related to NMR, in which quadrupolar nuclei are subjected to RF fields in the presence of a non-vanishing EFG. As far as its use for QIP is concerned, NQR shares most of the benefits of high-field NMR: reasonable sensitivity at room temperature, ease of manipulation by using standard control of RF pulses (duration, amplitude, phase) and, in favourable cases, relatively long transverse relaxation times. A clear-cut advantage of NQR over high-field NMR is that one does not need to use large magnetic fields in NQR experiments, which reduces tremendously the cost of NQR spectrometers, relative to commercial NMR spectrometers using superconducting magnets. On the negative side, NQR shows the same limitations as NMR with respect to the scalability of quantum computers and the problem of dealing with PPS in ensembles, as opposed to 'true' quantum computing systems that involve pure quantum states. Furthermore, the number of substances suitable for quantum computing applications via NQR is much more limited than in the NMR case, because NQR is observable only for quadrupolar nuclei placed in a site with a non-vanishing EFG.

Both zero-field NQR and Zeeman-perturbed NQR experiments are widely reported in the literature on quadrupolar nuclei, and more frequent examples involve the nuclides ^{35}Cl ($I = \frac{3}{2}$) and ^{14}N ($I = 1$) [37]. In zero-field or pure NQR, the Hamiltonian given in equation (2.1), describing the interaction between a nucleus with spin quantum number I and the EFG tensor at the site of the nucleus, is the only static interaction acting on the nuclear spin (disregarding other internal local fields). For an axially symmetric EFG tensor, the resulting energy levels are given by [37]

$$E_m = \frac{e^2 qQ\hbar}{4I(2I-1)}[m^2 - I(I+1)]. \tag{3.1}$$

These levels are thus degenerate in the quantum number m, with m and $-m$ states having the same energy. In the frequent case of half-integer spin quadrupolar nuclei, there are allowed transitions between the levels with $\Delta m = \pm 1$. Therefore, for $I = \frac{3}{2}$, for example, only one line appears in the pure NQR spectrum. When a small magnetic field is applied, the degeneracy is removed and more lines are observed. Again for $I = \frac{3}{2}$, a number of lines varying from one to four can be detected in Zeeman-perturbed NQR experiments, depending on the orientation of the applied magnetic field with respect to the PAS of the
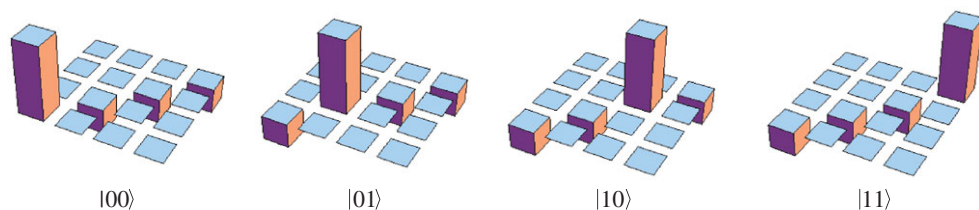
Figure 6. Simulated real parts of the density matrices corresponding to the four pseudo-pure states of the computational basis for zero-field NQR of a system of nuclei with $I = \frac{3}{2}$ in an axially symmetric EFG. Adapted from Possa *et al.* [18], copyright © 2011, with permission from Elsevier. (Online version in colour.)

EFG tensor (which is affected by sample orientation in experiments with single crystals) and on the type of excitation/detection scheme used (e.g. linearly or elliptically polarized RF pulses) [37–39].

Using circularly polarized RF pulses combined with double quantum excitation, Possa *et al.* [18] demonstrated the creation of two-qubit PPS and the implementation of the C-NOT gate in zero-field NQR of nuclei with $I = \frac{3}{2}$ in an axially symmetric EFG, taking ^{35}Cl nuclei in a single crystal of KClO$_3$ as an illustrative example. The required pulse sequences were detailed, and the results of typical experiments were simulated using a numerical procedure. Some of these results are shown in figure 6, where the real parts of the density matrices corresponding to the four PPS of the computational basis for a two-qubit system are exhibited. The creation of PPS for nuclei with $I = \frac{7}{2}$ in zero-field NQR was also discussed and the results of basic experiments were simulated. These results illustrate the potential of NQR as a simple and low-cost technique for the demonstration of quantum information principles and simulations of small quantum systems.

4. Relaxation behaviour of qubits implemented by quadrupolar spins

In the previous sections, it has been shown that three basic QIP steps—state preparation, quantum logical operations and state tomography—can be performed with quadrupolar nuclei. In the QIP context, systems of quadrupolar nuclei represent the so-called logical qubits. This is so, because for nuclear spin $I = \frac{3}{2}$ the eigenvectors of the Zeeman plus quadrupolar terms are $|\frac{3}{2}\rangle$, $|\frac{1}{2}\rangle$, $|-\frac{1}{2}\rangle$ and $|-\frac{3}{2}\rangle$, which can be labelled as $|00\rangle$, $|01\rangle$, $|10\rangle$ and $|11\rangle$, corresponding to a two-qubit system. In this regard, in quadrupolar systems, more than one bit of quantum information is stored in a single entity. This contrasts with the more usual NMR implementations using spin $\frac{1}{2}$ systems, where each spin represents one qubit, the so-called physical qubit. This leads to questions about to what extent the quadrupolar spin qubits are equivalent to the spin $\frac{1}{2}$ qubits. However, in order to provide a more detailed comparison between the systems, we need to consider a more general picture, in which the evolution of the quantum state and its interaction with the thermal environment are also taken into account. Thus,

this section is devoted to a brief review of the interaction of quadrupolar spins with their typical thermal environment in order to highlight some unique features of these systems in relation to spin $\frac{1}{2}$ systems.

(a) Action of the environment on a quadrupolar spin $\frac{3}{2}$ system

Like any quantum system, quantum states prepared with quadrupolar spins are also prone to decoherence and damping owing to interaction with their local environment. Internal molecular or atomic motions induce random fluctuations in the EFG at the position of the nucleus, which produce spin relaxation [40,41]. In the QIP context, the random fluctuations can be seen as a source of noise, which causes decoherence and energy dissipation, being mapped by proper non-unitary operators [24]. In both descriptions, it is crucial to understand how the environment affects the states, i.e. how the system density matrix behaves under the action of the EFG random fluctuations.

The modelling of the motion-induced EFG fluctuations can become rather complex because, besides the quadrupolar interaction parameters, it also depends on structural and dynamic features of the local environment around the relaxing spins [40,42]. In the most usual analysis, this effect is encoded in a set of reduced spectral densities, J_n, which depend on the rates of motion, nucleus frequency and geometry [40,42,43]. Considering the quadrupolar interaction as the only source of spin relaxation (pure quadrupolar relaxation), Jaccard *et al.* [44] show that the relaxation of a spin $\frac{3}{2}$ system can be described by three reduced spectral densities, J_0, J_1 and J_2, with the explicit expressions relating the spectral densities and the molecular parameter given in Auccaise *et al.* [11]. Using the spectral densities, the relaxation of each element $\Delta\rho_{ij}$ of the traceless deviation matrix can be predicted by using the well-known Redfield formalism [11,22], leading to

$$
\left.
\begin{aligned}
\Delta\rho_{01}(t) &= \tfrac{1}{2}[\Delta\rho_{01}^0 + \Delta\rho_{23}^0 + (\Delta\rho_{01}^0 - \Delta\rho_{23}^0)\,e^{-2CJ_2 t}]\,e^{-C(J_0+J_1)t}, \\
\Delta\rho_{02}(t) &= \tfrac{1}{2}[\Delta\rho_{02}^0 + \Delta\rho_{13}^0 + (\Delta\rho_{02}^0 - \Delta\rho_{13}^0)\,e^{-2CJ_1 t}]\,e^{-C(J_0+J_2)t}, \\
\Delta\rho_{13}(t) &= \tfrac{1}{2}[\Delta\rho_{02}^0 + \Delta\rho_{13}^0 - (\Delta\rho_{02}^0 - \Delta\rho_{13}^0)\,e^{-2CJ_1 t}]\,e^{-C(J_0+J_2)t}, \\
\Delta\rho_{23}(t) &= \tfrac{1}{2}[\Delta\rho_{01}^0 + \Delta\rho_{23}^0 - (\Delta\rho_{01}^0 - \Delta\rho_{23}^0)\,e^{-2CJ_2 t}]\,e^{-C(J_0+J_1)t}, \\
\Delta\rho_{03}(t) &= \Delta\rho_{03}^0\,e^{-C(J_1+J_2)t}, \\
\Delta\rho_{12}(t) &= \Delta\rho_{12}^0\,e^{-C(J_1+J_2)t}, \\
\Delta\rho_{00}(t) &= \tfrac{3}{2} - \tfrac{1}{4}[R_1\,e^{-2C(J_1+J_2)t} - R_2\,e^{-2CJ_2 t} - R_3\,e^{-2CJ_1 t}], \\
\Delta\rho_{11}(t) &= \tfrac{1}{2} + \tfrac{1}{4}[R_1\,e^{-2C(J_1+J_2)t} + R_2\,e^{-2CJ_2 t} - R_3\,e^{-2CJ_1 t}], \\
\Delta\rho_{22}(t) &= -\tfrac{1}{2} + \tfrac{1}{4}[R_1\,e^{-2C(J_1+J_2)t} - R_2\,e^{-2CJ_2 t} + R_3\,e^{-2CJ_1 t}]
\end{aligned}
\right\}
\tag{4.1}
$$

and
$$
\Delta\rho_{33}(t) = -\tfrac{3}{2} - \tfrac{1}{4}[R_1\,e^{-2C(J_1+J_2)t} + R_2\,e^{-2CJ_2 t} + R_3\,e^{-2CJ_1 t}],
$$

where $\Delta\rho_{ij}$ stands for the deviation matrix elements with the index values $i,j = 0,1,2,3$ corresponding to the quantum number $m = +\frac{3}{2}, +\frac{1}{2}, -\frac{1}{2}, -\frac{3}{2}$ indexing the energy levels. The superscript 0 stands for the initial value of each deviation matrix element and R_i ($i = 1, 2, 3$) are constant coefficients. The parameter

J. Teles et al.

C is proportional to the quadrupolar coupling frequency $\nu_Q = \omega_Q/2\pi$ and can be obtained from the NMR spectrum [11,42]. From equation (4.1), it can be seen that the relaxation of the elements $\Delta\rho_{00}, \Delta\rho_{11}, \Delta\rho_{22}, \Delta\rho_{33}$ (populations) and $\Delta\rho_{03}, \Delta\rho_{12}$ (triple quantum coherences) relates only to the spectral densities J_1 and J_2, whereas the remaining elements $\Delta\rho_{01}, \Delta\rho_{02}, \Delta\rho_{13}, \Delta\rho_{23}$ depend also on J_0.

The set of equations mentioned earlier predicts the action of the environment (modelled in the reduced spectral densities) on each element $\Delta\rho_{m,n}$; so the spectral densities can be experimentally obtained by monitoring the evolution of the density matrix elements. This is achieved by preparing an initial state, which is allowed to evolve under the action of the environment for a period τ, and then carrying out QST to obtain the evolved deviation matrix $\Delta\rho(\tau)$. This procedure is repeated for various values of τ, which is incremented stepwise. To avoid the oscillations imposed by the evolution under the quadrupolar interaction, the τ increments are set to multiples of $2\pi/\omega_Q$. The decay due to the magnetic field inhomogeneity is eliminated by placing a π pulse in the middle of the total evolution period, as depicted in figure 7*a*.

Figure 7*b* shows the decay of each deviation matrix element for a full superposition PPS, $|\mathrm{sup}\rangle \equiv \frac{1}{2}(|00\rangle + |01\rangle + |10\rangle + |11\rangle)$, implemented in the ^{23}Na nuclear spin system ($I = \frac{3}{2}$) described in §5. The experimental data were fitted by equation (4.1), using the procedure described in Auccaise *et al.* [11]. With $C = (11.7 \pm 1.4) \times 10^9\,\mathrm{s}^{-2}$, obtained from the NMR spectrum [11,42], the reduced spectral densities were found to be $J_0 = (17.0 \pm 3.9) \times 10^{-9}\,\mathrm{s}$, $J_1 = (3.0 \pm 0.5) \times 10^{-9}\,\mathrm{s}$, $J_2 = (3.4 \pm 0.5) \times 10^{-9}\,\mathrm{s}$.

As detailed in Souza *et al.* [13], the relaxation in this spin $\frac{3}{2}$ system can alternatively be modelled by a quantum circuit treatment. In this treatment, the effect of the environment on the spin system is taken into account by considering the main system S as being composed of N subsystems that interact with the environment through quantum channels. These quantum channels are usually classified as global channels, in which all subsystems interact with the same environment, and local channels, in which each subsystem interacts with its own environment [23,24]. Some examples of quantum channels are: generalized amplitude damping (GAD), generalized phase damping (GPD), bit-flip, phase-flip and depolarizing channels. Once the quantum channels contributing to the system–environment interaction are defined, the density operator under the influence of the environment (ρ') is calculated from the initial density matrix (ρ) as

$$\rho' = \sum_{k...m} E_k^1 \otimes \cdots \otimes E_m^N \rho E_k^{1\dagger} \otimes \cdots \otimes E_m^{N\dagger}, \tag{4.2}$$

where E_i^j are the well-known Kraus operators, defined for a given quantum channel [23,24].

In the quadrupolar spin $\frac{3}{2}$ system described by equation (4.1), the elements $\Delta\rho_{00}$, $\Delta\rho_{11}$, $\Delta\rho_{22}$, $\Delta\rho_{33}$ are uncoupled and depend only on the spectral densities J_1 and J_2. This feature makes it possible to describe the energy dissipation of the system by two dissipative GAD channels acting on each qubit separately that can be represented by the successive action of the following Kraus operators:

$$E_0 = \sqrt{\gamma}\begin{pmatrix} 1 & 0 \\ 0 & \sqrt{1-p} \end{pmatrix}, \quad E_1 = \sqrt{\gamma}\begin{pmatrix} 0 & \sqrt{p} \\ 0 & 0 \end{pmatrix}$$
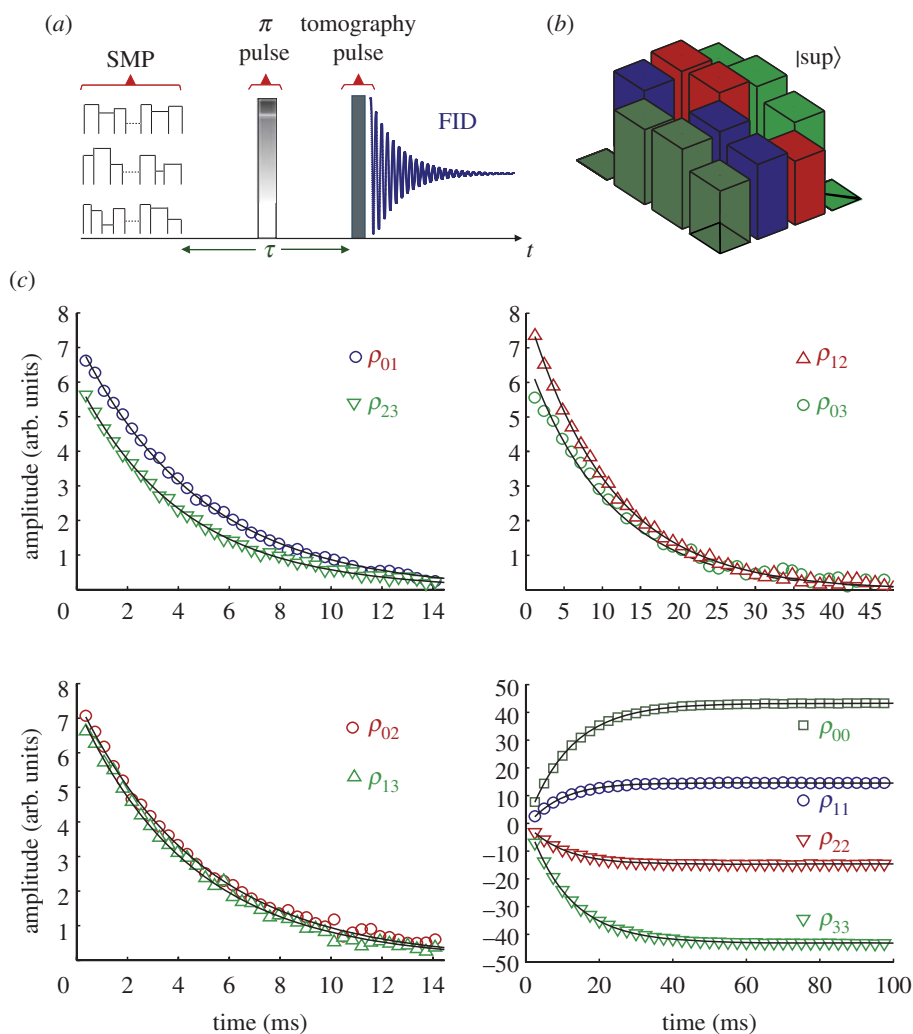
Figure 7. (*a*) Basic pulse sequence used to probe the relaxation of the deviation matrix elements. (*b*) Bar representation of the deviation matrix corresponding to the state |sup⟩ (real part only). The horizontal axes follow the same convention of figure 4. (*c*) Experimental data (symbols) and curves fitted by equation (4.1) (lines) showing the relaxation of the deviation matrix elements shown in (*b*). Adapted from Auccaise *et al.* [11], copyright 2011, with permission from Elsevier. (Online version in colour.)

and

$$E_2 = \sqrt{1-\gamma} \begin{pmatrix} \sqrt{1-p} & 0 \\ 0 & 1 \end{pmatrix}, \quad E_3 = \sqrt{1-\gamma} \begin{pmatrix} 0 & 0 \\ \sqrt{p} & 0 \end{pmatrix},$$

where γ represents the probability of the system decaying from the excited state |1⟩ to the ground state |0⟩ and p is the probability of finding the system at thermal equilibrium in its ground state.

Another feature of equation (4.1) is that only the elements $\Delta\rho_{01}$, $\Delta\rho_{02}$, $\Delta\rho_{13}$, $\Delta\rho_{23}$ depend on J_0, showing that the Bell states are not affected by the phase damping channel [13]. The decoherence of the other elements is dictated by a GPD channel acting simultaneously on both qubits. The Kraus operators associated with this GPD channel are given by

$$E_0 = \sqrt{1-\lambda} \begin{bmatrix} 1 & 0 & 0 & 0 \\ 0 & -1 & 0 & 0 \\ 0 & 0 & -1 & 0 \\ 0 & 0 & 0 & 1 \end{bmatrix} \tag{4.3}$$

and

$$E_1 = \sqrt{\lambda} \begin{bmatrix} 1 & 0 & 0 & 0 \\ 0 & 1 & 0 & 0 \\ 0 & 0 & 1 & 0 \\ 0 & 0 & 0 & 1 \end{bmatrix}. \tag{4.4}$$

By using both the GAD and GPD channels, a set of equations equivalent to (4.1) but parametrized by p, γ and λ can be obtained, and by fitting them to the experimental data, the Kraus operators can be found in terms of the reduced spectral densities [13].

In summary, the representation of the quadrupolar spin $\frac{3}{2}$ relaxation in terms of the Kraus operators shows directly that, in this two-qubit system, the environment acts globally; i.e. simultaneously on both qubits. This feature can also be derived directly from equations (4.1) by calculating the magnetization associated to each logical qubit using a partial trace operation [11].

A final remark about the relaxation properties concerns the nature of the environment. In the treatment based on the Redfield formalism, the environment is assumed to be classical. However, it was shown recently that the Redfield formalism for treating the dissipative dynamics of a time-dependent quantum system coupled to a classical environment leads to the same result as the master equation approach with the environment treated quantum mechanically [45]. This supports the use of the traditional Redfield approach in the treatment of NMR systems for QIP.

(b) Quantum correlations in quadrupolar NMR systems

For many years, quantum entanglement was assumed to be an essential resource in QIP [46–49]. Since the early days of NMR QIP, it was also clear that the systems based on a bulk liquid-state NMR with less than 12 qubits do not present true entanglement [50,51]. Despite that, NMR systems continued to be used widely as test benches that demonstrated the speed-up of many quantum operations, although the origin of the quantum correlations that produced such a speed-up was unclear. This scenario started to change with the first reports that the speed-up of many quantum process could be achieved without entanglement; in other words, it could be produced by quantum correlation in separable states [52,53]. In this regard, Ollivier & Zurek [54] proposed the so-called quantum discord as a measure of quantum correlations of separable states. The quantum discord represents a measurement of the gap between quantum and classical information theory, expressed as the difference between the mutual information and classical correlation, which can be calculated from the density

matrix of a given quantum system [54]. Interestingly, there is no requirement about the purity of the quantum state in the calculation of the quantum discord, so it can be obtained even for highly mixed states.

Considering a typical two-qubit NMR density matrix, it can be shown that both the mutual information and classical correlations can be obtained directly from the deviation matrix $\Delta\rho$ [14], so that it is possible to calculate the quantum discord directly from experimentally tomographed NMR deviation matrices. By this means, the quantum discord was experimentally measured for the first time in NMR with the quadrupolar spin $\frac{3}{2}$ systems described in §5, in an X-type PPS (prepared using the SMP method) by the following deviation matrix:

$$\Delta\rho = \begin{bmatrix} a & 0 & 0 & f \\ 0 & b & e & 0 \\ 0 & e^* & c & 0 \\ f^* & 0 & 0 & d \end{bmatrix} \tag{4.5}$$

and

$$\Delta\rho \approx \begin{bmatrix} c_3 & 0 & 0 & (c_1 - c_2) \\ 0 & -c_3 & (c_1 + c_2) & 0 \\ 0 & (c_1 + c_2)^* & -c_3 & 0 \\ (c_1 - c_2)^* & 0 & 0 & c_3 \end{bmatrix}, \tag{4.6}$$

where $a = 0.4679$, $b = -0.5066$, $c = -0.5447$, $d = 0.4872$, $e = 0.7645 + \text{i}0.0398$ and $f = 0.5853 - \text{i}0.009$. The values of a, b, c, d, e and f were chosen to have $a \approx d \approx -b \approx -c = c_3$, $(e + f)/2 \approx c_1$ and $(e - f)/2 \approx -c_2$, so that equation (4.6) can be approximated to the form with $|c_1| > |c_3|, |c_2|$. The reason for this choice will become clear in the following discussion. The quantum correlation (measured by the quantum discord) for this state was found to be about (2.0 ± 0.2) in units of $\epsilon/\ln(2)$. Note that, despite being a rather small number ($\epsilon \approx 10^{-5}$), this value is beyond the NMR detection limit because only the deviation density matrix, from which the quantum correlation is calculated, is detected in NMR measurements. This demonstrates the existence of quantum correlations of separable states in the spin $\frac{3}{2}$ system under consideration [14].

The effect of the environment on the quantum correlations was also experimentally monitored [14], by preparing the state (4.5) and characterizing its evolution by following the procedure described in §4a. The mutual information, classical and quantum correlations were then calculated for each step of the evolution. Assuming the same initial state and the reduced spectral densities given in §4a, the correlations were also calculated theoretically. Both experimental and theoretical plots of the correlations against the evolution time τ are shown in figure 8a. It can be observed that all correlations decay monotonically with a rate determined by the spectral densities (or equivalently the characteristic relaxation times of the system).

In Auccaise *et al.* [25], an X-type deviation matrix, with a, b, c, d and f chosen in order to have $|c_1|, |c_2| > |c_3|$, was prepared using a two-qubit spin $\frac{1}{2}$ system implemented by ^{13}C and ^{1}H nuclei in a chloroform sample. The evolution of the correlations was also monitored by a similar procedure [25]. The results are reproduced in figure 8b. In this case, instead of a monotonic decay, an abrupt change in the decay rates of the correlations was observed at a certain value of τ. This phenomenon, usually referred to as a sudden transition, was first
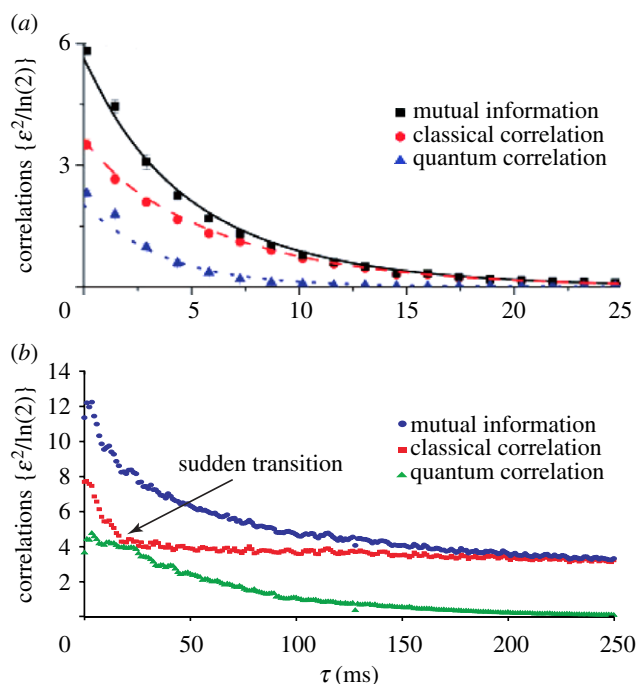
Figure 8. (*a*) Evolution of the mutual information, quantum and classical correlations measured for the *X*-type deviation matrix implemented in a quadrupolar spin $\frac{3}{2}$ system. The initial deviation matrix is given in equation (4.5) with the coefficients *a*, *b*, *c*, *d* and *f* given in the text. (*b*) Evolution of the mutual information, quantum and classical correlations measured for the *X*-type deviation matrix implemented in a 2-coupled spin $\frac{1}{2}$ system. Adapted from [14,25], copyright 2011, with permission from American Physical Society. (Online version in colour.)

theoretically predicted in Maziero *et al.* [55], where it was shown that, for an *X*-type deviation matrix with $|c_1| > |c_3|, |c_2|$ or $|c_1|, |c_2| > |c_3|$, the classical correlation initially decays exponentially up to a certain time and then remains constant, while the quantum correlation suddenly increases its decay rate at the same instant. This was also experimentally measured in an optical setup where the qubits were encoded in the photon polarization and the phase damping channel was simulated in a controlled way by a birefringent medium [56]. The exact origin of this peculiar behaviour of the correlations is beyond the scope of this study and can be found in more detail in the earlier-mentioned references. However, in figure 8*a*,*b*, the initial deviation matrices fulfil the conditions for a sudden transition, but it is observed only for the ^{13}C–^{1}H spin $\frac{1}{2}$ system. This results from the intrinsic difference between these two-qubit systems in terms of interaction with the environment. The sudden change in behaviour is expected to occur in a two-qubit system where each qubit interacts with its own environment, with local amplitude and phase damping channels. This condition is fulfilled for the spin $\frac{1}{2}$ system, where the ^{13}C and ^{1}H nuclei are separate physical entities. In contrast, as shown in Souza *et al.* [13] and discussed in §4*a*, in the spin $\frac{3}{2}$ system the phase damping channel is global and no sudden change in behaviour is expected in this situation [14].

In summary, quadrupolar spin systems (particularly the spin $\frac{3}{2}$ system treated as an example here) can be used in QIP to implement logical qubits, being equivalent to coupled spin $\frac{1}{2}$ systems in terms of performing quantum operations. However, even with the same qubit encoding if the interaction of the qubits with the environment is taken into consideration, quadrupolar nuclei and coupled spin $\frac{1}{2}$ nuclei may behave significantly differently because of the distinct internal spin Hamiltonians. This distinct behaviour has been revealed in several contexts and some of them were reviewed briefly here. This feature is also manifested when these NMR systems are used to simulate other quantum systems. For example, while a coupled spin $\frac{1}{2}$ system was used to simulate the evolution of fermionic particles in a harmonic oscillator potential [23], a spin $\frac{3}{2}$ system was used to mimic a Bose–Einstein condensate [57].

5. Experimental

The experimental demonstrations presented earlier with the spin $\frac{3}{2}$ system were carried out on ^{23}Na nuclei dissolved in a lyotropic liquid crystal prepared with 20.9 wt% sodium dodecylsulphate (SDS) (95% pure), 3.7 wt% decanol and 75.4 wt% deuterium oxide, following the procedure described elsewhere [42]. The ^{23}Na NMR experiments were performed at room temperature in a 9.4 T-Varian Inova spectrometer with a 7 mm solid-state NMR probe head. A small sample volume occupying one-third of the uniform B_1 field region of the RF coil was used. The probe head was chosen for its solenoidal design, which is very efficient in the production of strong RF fields. This feature is important for the implementation of the hard non-selective pulses used in the tomography method described herein. However, as a consequence of the trade-off between intensity and homogeneity, the RF field is significantly inhomogeneous in the sample region. For this reason, a small spherical glass bulb was used to hold the liquid crystal. Even so, a good signal-to-noise ratio was obtained owing to the coil efficiency. Another advantage of the spherical form of the sample holder is that B_0 field homogenization is facilitated [58]. The glass bulb was positioned inside the 7 mm rotor in its standard magic angle orientation.

6. Conclusions

Quadrupolar nuclei in the presence of an EFG have been shown to be an important experimental system for QIP studies by NMR and NQR in a variety of materials. As an example, we have demonstrated its use in preparing PPS, implementing logic gates and performing quantum algorithms. The success of these steps can be clearly appreciated from the experimental results obtained for the Grover algorithm implementation which, despite a not so high fidelity obtained in some instances ($F \gtrsim 0.8$), exhibited the fully expected periodic and global behaviour. An important question regarding the quadrupolar nuclei, with respect to their use as qubits, is how their dynamics differs from the single qubit spin $\frac{1}{2}$ systems. This is especially important when studying the relaxation processes of the nuclear ensemble and their effects on the quantum nature of the information contained in the system. The results on relaxation and quantum

correlations discussed in this work showed that the nature of the system–environment interaction, which defines specific quantum channels for relaxation, is crucial for the observation of quantum phenomena such as the sudden transition in the quantum correlations. All experiments shown in this work benefitted from an extremely fast QST technique for quadrupolar nuclei that uses only short hard RF pulses. Particularly, in the SDS liquid crystal sample, the tomography pulses took around one-thousandth of the shortest transverse relaxation times. Therefore, the reading stages in the pulse sequences contributed a negligible coherence loss and dissipation of the computational quantum states.

Further possible work with the quadrupolar systems includes experimental implementation of the NQR proposals expounded here and combined use of the dipolar and quadrupolar interactions in solid-state NMR (because the highest available spin gives rise to at most three qubits). One recent study that involved quadrupolar effects in magnetic materials [59] is worth mentioning. In that study, relatively high-resolution spectra were obtained from a powdered sample of the intermetallic compound $GdAl_2$ in the magnetically ordered state. The attractive characteristic of such a system is that the main magnetic field, which characterizes the NMR regime, is produced internally by the sample. As in the NQR case, this is a cheaper and more compact experimental setup, because the large superconducting magnets are avoided. However, the strong RF inhomogeneities that are typical in these conducting materials are an important obstacle that could be tackled by using single crystal samples, for example.

References

1 Khitrin, A. K. & Fung, B. M. 2000 Nuclear magnetic resonance quantum logic gates using quadrupolar nuclei. *J. Chem. Phys.* **112**, 6963–6965. (doi:10.1063/1.481293)

2 Sinha, N., Mahesh, T. S., Ramanathan, K. V. & Kumar, A. 2001 Toward quantum information processing by nuclear magnetic resonance: pseudopure states and logical operations using selective pulses on an oriented spin $\frac{3}{2}$ nucleus. *J. Chem. Phys.* **114**, 4415–4420. (doi:10.1063/1.1346645)

3 Kampermann, H. & Veeman, W. S. 2002 Quantum computing using quadrupolar spins in solid state NMR quantum information processing. *Quantum Inf. Process.* **1**, 327–344. (doi:10.1023/A:1023461628937)

4 Murali, K. V. R. M., Sinha, N., Mahesh, T. S., Levitt, M. H., Ramanathan, K. V. & Kumar, A. 2002 Quantum-information processing by nuclear magnetic resonance: experimental implementation of half-adder and subtractor operations using an oriented spin-$\frac{7}{2}$ system. *Phys. Rev. A* **66**, 022313. (doi:10.1103/PhysRevA.66.022313)

5 Das, R. & Kumar, A. 2003 Use of quadrupolar nuclei for quantum information processing by nuclear magnetic resonance: implementation of a quantum algorithm. *Phys. Rev. A* **68**, 032304. (doi:10.1103/PhysRevA.68.032304)

6 Bonk, F. A., Sarthour, R. S., deAzevedo, E. R., Bulnes, J. D., Mantovani, G. L., Freitas, J. C. C., Bonagamba, T. J., Guimaraes, A. P. & Oliveira, I. S. 2004 Quantum-state tomography for quadrupole nuclei and its application on a two-qubit system. *Phys. Rev. A* **69**, 042322. (doi:10.1103/PhysRevA.69.042322)

7 Chuang, I. L., Gershenfeld, N., Kubinec, M. G. & Leung, D. W. 1998 Bulk quantum computation with nuclear magnetic resonance: theory and experiment. *Proc. R. Soc. Lond. A* **454**, 447–467. (doi:10.1098/rspa.1998.0170)

8 Long, G. L., Yan, H. Y. & Sun, Y. 2001 Analysis of density matrix reconstruction in NMR quantum computing. *J. Opt. B* **3**, 376–381. (doi:10.1088/1464-4266/3/6/305)

9 Chuang, I. L., Gershenfeld, N. & Kubinec, M. G. 1998 Experimental implementation of fast quantum searching. *Phys. Rev. Lett.* **80**, 3408–3411. (doi:10.1103/PhysRevLett.80.3408)

10 Teles, J., deAzevedo, E. R., Auccaise, R., Sarthour, R. S., Oliveira, I. S. & Bonagamba, T. J. 2007 Quantum state tomography for quadrupolar nuclei using global rotations of the spin system. *J. Chem. Phys.* **126**, 154506. (doi:10.1063/1.2717179)

11 Auccaise, R., Teles, J., Sarthour, R. S., Bonagamba, T. J., Oliveira, I. S. & deAzevedo, E. R. 2008 A study of the relaxation dynamics in a quadrupolar NMR system using quantum state tomography. *J. Magn. Reson.* **192**, 17–26. (doi:10.1016/j.jmr.2008.01.009)

12 Gavini-Viana, A., Souza, A. M., Soares-Pinto, D. O., Teles, J., Sarthour, R. S., deAzevedo, E. R., Bonagamba, T. J. & Oliveira, I. S. 2010 Normalization procedure for relaxation studies in NMR quantum information processing. *Quantum Inf. Process.* **9**, 575–589. (doi:10.1007/s11128-009-0158-1)

13 Souza, A. M., Gavini-Viana, A., Auccaise, R., deAzevedo E. R., Bonagamba, T. J., Sarthour, R. S. & Oliveira, I. S. 2010 Nuclear spin $\frac{3}{2}$ electric quadrupole relaxation as a quantum computation process. *Quantum Inf. Comput.* **10**, 0653–0668. (http://arxiv.org/abs/1105.2539)

14 Soares-Pinto, D. O., Celeri, L. C., Auccaise, R., Fanchini, F. F., deAzevedo, E. R., Maziero, J., Bonagamba, T. J. & Serra, R. M. 2010 Nonclassical correlation in NMR quadrupolar systems. *Phys. Rev. A* **81**, 062118. (doi:10.1103/PhysRevA.81.062118)

15 Soares-Pinto, D. O., Teles, J., Souza, A. M., deAzevedo, E. R., Sarthour, R. S., Bonagamba, T. J., Reis, M. S. & Oliveira, I. S. 2011 Writing electronic ferromagnetic states in a high-temperature paramagnetic nuclear spin system. *Int. J. Quantum Inf.* **9**, 1047–1056. (doi:10.1142/S021974991100785X)

16 Furman, B., Goren, S. D., Meerovich, V. M. & Sokolovsky, V. L. 2002 Two qubits in pure nuclear quadrupole resonance. *J. Phys. Condens. Matter* **14**, 8715–8723. (doi:10.1088/0953-8984/14/37/308)

17 Furman, G. B. & Goren, S. D. 2002 Pure NQR quantum computing. *Z. Naturforsch. A* **57**, 315–319.

18 Possa, D., Gaudio, A. C. & Freitas, J. C. C. 2011 Numerical simulation of NQR/NMR experiments: applications in quantum computing. *J. Magn. Reson.* **209**, 250–260. (doi:10.1016/j.jmr.2011.01.020)

19 Weber, M. J. & Hahn, E. L. 1960 Selective spin excitation and relaxation in nuclear quadrupole resonance. *Phys. Rev.* **120**, 365–375. (doi:10.1103/PhysRev.120.365)

20 Miller, J. B., Suits, B. H. & Garroway, A. N. 2001 Circularly polarized RF magnetic fields for spin-1 NQR. *J. Magn. Reson.* **151**, 228–234. (doi:10.1006/jmre.2001.2366)

21 Eles, P. T. & Michal, C. A. 2005 Crossed-coil detection of two-photon excited nuclear quadrupole resonance, *J. Magn. Reson.* **175**, 201–209. (doi:10.1016/j.jmr.2005.04.006)

22 Redfield, A. G. 1957 On the theory of relaxation processes. *IBM J. Res. Dev.* **1**, 19–26. (doi:10.1147/rd.11.0019)

23 Nielsen, A. E. & Chuang, I. L. 2000 *Quantum computation and quantum information.* Cambridge, UK: Cambridge University Press.

24 Breuer H. P. & Petruccione F. 2007 *The theory of open quantum systems.* New York, NY: Oxford University Press.

25 Auccaise, R., Soares-Pinto, D. O., Celeri, L. C., deAzevedo, E. R., Maziero, J., Souza, A., Bonagamba, T. J., Sarthour, R. S., Oliveira, I. S. & Serra, R. M. 2011 Environment-induced sudden transition in quantum discord dynamics. *Phys. Rev. Lett.* **107**, 140403. (doi:10.1103/PhysRevLett.107.140403)

26 Gershenfeld, N. A. & Chuang, I. L. 1997 Bulk spin–resonance quantum computation. *Science* **275**, 350–356. (doi:10.1126/science.275.5298.350)

27 Cory, D. G., Fahmy, A. F. & Havel, T. F. 1997 Ensemble quantum computing by NMR spectroscopy *Proc. Natl Acad. Sci. USA* **94**, 1634–1639. (doi:10.1073/pnas.94.5.1634)

28 Waugh, J. S. 1996 Average Hamiltonian theory. In *Encyclopedia of nuclear magnetic resonance* (eds D. M. Grant & R. K. Harris), pp. 849–854. Chichester, UK: Wiley.

29 Wokaun, A. & Ernst, R. R. 1977 Selective excitation and detection in multilevel spin systems: application of single transition operators. *J. Chem. Phys.* **67**, 1752–1758. (doi:10.1063/1.435038)

30 Vega, S. & Pines, J. 1977 Operator formalism for double quantum NMR. *J. Chem. Phys.* **66**, 5624–5644. (doi:10.1063/1.433884)

31 Fortunato, E. M., Pravia, M. A., Boulant, N., Teklemariam, G., Havel, T. F. & Cory, D. G. 2002 Design of strongly modulating pulses to implement precise effective Hamiltonians for quantum information processing. *J. Chem. Phys.* **116**, 7599–7606. (doi:10.1063/1.1465412)

32 Varshalovich, D., Moskalev, A. & Khersonskii, V. 1988 *Quantum theory of angular momentum.* Singapore: World Scientific.

33 Grover, L. K. 1996 A fast quantum mechanical algorithm for database search. In *STOC '96 Proc. 28th Annual ACM Symp. on Theory of Computing*, pp. 212–219. New York, NY: ACM. (doi:10.1145/237814.237866)

34 Jones, J. A., Mosca, M. & Hansen, R. H. 1998 Implementation of a quantum search algorithm on a quantum computer. *Nature* **393**, 344–346. (doi:10.1038/30687)

35 Ermakov, V. L. & Fung B. M. 2002 Experimental realization of a continuous version of the Grover algorithm. *Phys. Rev. A* **66**, 042310. (doi:10.1103/PhysRevA.66.042310)

36 Oliveira, I. S., Bonagamba, T. J., Sarthour, R. S., Freitas, J. C. C. & deAzevedo, E. R. 2007 *NMR quantum information processing.* Amsterdam, The Netherlands: Elsevier.

37 Das, T. P. & Hahn, E. L. 1958 *Nuclear quadrupole resonance spectroscopy.* New York, NY: Academic Press Inc.

38 Bain, A. D. & Khasawneh, M. 2004 From NQR to NMR: the complete range of quadrupole interactions. *Concepts Magn. Reson. A* **22**, 69–78. (doi:10.1002/cmr.a.20013)

39 Zeldes, H. & Livingston, R. 1957 Zeeman effect on the quadrupole spectra of sodium, potassium, and barium chlorates. *J. Chem. Phys.* **26**, 1102–1106. (doi:10.1063/1.1743479)

40 Abragam, A. 1978 *The principles of nuclear magnetism.* New York, NY: Oxford University Press.

41 Sarthour, R. S., deAzevedo, E. R., Bonk, F. A., Vidoto, E. L. G., Bonagamba, T. J., Guimaraes, A. P., Freitas, J. C. C. & Oliveira, I. S. 2003 Relaxation of coherent states in a two-qubit NMR quadrupole system. *Phys. Rev. A* **68**, 022311. (doi:10.1103/PhysRevA.68.022311)

42 Radley, K., Reeves, L. W. & Tracey, A. S. 1976 Effect of counterion substitution on type and nature of nematic lyotropic phases from nuclear magnetic resonance studies. *J. Phys. Chem.* **80**, 174–182. (doi:10.1021/j100543a018)

43 Lipari, G. & Szabo, A. 1982 Model-free approach to the interpretation of nuclear magnetic resonance relaxation in macromolecules. *J. Am. Chem. Soc.* **104**, 4546–4559. (doi:10.1021/ja00381a009)

44 Jaccard, G., Wimperis, S. & Bodenhausen, G. 1986 Multiple-quantum NMR spectroscopy of $S = \frac{3}{2}$ spins in isotropic phase: a new probe for multiexponential relaxation. *J. Chem. Phys.* **85**, 6282–6293. (doi:10.1063/1.451458)

45 Soares-Pinto, D. O., Moussa, M. H. Y., Maziero, J., deAzevedo, E. R., Bonagamba, T. J., Serra, R. M. & Celeri, L. C. 2011 Equivalence between Redfield- and master-equation approaches for a time-dependent quantum system and coherence control. *Phys. Rev. A* **83**, 062336. (doi:10.1103/PhysRevA.83.062336)

46 Werner, R. F. 1989 Quantum states with Einstein–Podolsky–Rosen correlations admitting a hidden-variable model. *Phys. Rev. A* **40**, 4277–4281. (doi:10.1103/PhysRevA.40.4277)

47 Bell, J. S. 1988 *Speakable and unspeakable in quantum mechanics.* Cambridge, UK: Cambridge University Press.

48 Einstein, A., Podolsky, B. & Rosen, N. 1935 Can quantum-mechanical description of physical reality be considered complete? *Phys. Rev.* **47**, 777–780. (doi:10.1103/PhysRev.47.777)

49 Horodecki, R., Horodecki, P., Horodecki, M. & Horodecki, K. 2009 Quantum entanglement. *Rev. Mod. Phys.* **81**, 865–942. (doi:10.1103/RevModPhys.81.865)

50 Braunstein, S. L., Caves, C. M., Jozsa, R., Linden, N., Popescu, S. & Schack, R. 1999 Separability of very noisy mixed states and implications for NMR quantum computing. *Phys. Rev. Lett.* **83**, 1054–1057. (doi:10.1103/PhysRevLett.83.1054)

51 Linden, N. & Popescu, S. 2001 Good dynamics versus bad kinematics: is entanglement needed for quantum computation? *Phys. Rev. Lett.* **87**, 047901. (doi:10.1103/PhysRevLett.87.047901)

52 Datta, A., Shaji, A. & Caves, C. M. 2008 Quantum discord and the power of one qubit. *Phys. Rev. Lett.* **100**, 050502. (doi:10.1103/PhysRevLett.100.050502)

53 Lanyon, B. P., Barbieri, M., Almeida, M. P. & White, A. G. 2008 Experimental quantum computing without entanglement. *Phys. Rev. Lett.* **101**, 200501. (doi:10.1103/PhysRevLett. 101.200501)

54 Ollivier, H. & Zurek, W. H. 2001 Quantum discord: a measure of the quantumness of correlations. *Phys. Rev. Lett.* **88**, 017901. (doi:10.1103/PhysRevLett.88.017901)

55 Maziero, J., Céleri, L. C., Serra, R. M. & Vedral, V. 2009 Classical and quantum correlations under decoherence. *Phys. Rev. A* **80**, 044102. (doi:10.1103/PhysRevA.80.044102)

56 Xu, J.-S., Xu, X.-Y., Li, C.-F., Zhang, C.-J., Zou, X.-B. & Guo, G.-C. 2010 Experimental investigation of classical and quantum correlations under decoherence. *Nat. Commun.* **1**, 7. (doi:10.1038/ncomms1005)

57 Auccaise, R., Teles, J., Bonagamba, T. J., Oliveira, I. S., deAzevedo, E. R. & Sarthour, R. S. 2009 NMR quadrupolar system described as Bose–Einstein-condensate-like system. *J. Chem. Phys.* **130**, 144501. (doi:10.1063/1.3106044)

58 Teles, J., Garrido, C. E. & Tannus, A. 2004 A convenient procedure for magnetic field homogeneity evaluation. *J. Phys. D* **37**, 1877–1880. (doi:10.1088/0022-3727/37/14/001)

59 Tozoni, J. R., Teles, J., Auccaise, R., Oliveira-Silva, R., Rivera-Ascona, C., Vidoto, E. L. G., Guimaraes, A. P., Oliveira, I. S. & Bonagamba, T. J. 2011 Multi-quantum echoes in $GdAl_2$ zero-field high-resolution NMR. *J. Magn. Reson.* **212**, 265–273. (doi:10.1016/j.jmr.2011.07.003)